# The morphology and hydrocollapse behavior of loess-like deposits in the Mount Moorosi village in Lesotho

Monica Damane, Denis Kalumba[1], Laxmee Sobhee-Beetul[2]
*Department of civil engineering, University of Cape Town, Cape Town, South Africa,*
*dmnmon001@myuct.ac.za, denis.kalumba@uct.ac.za[1] and* sbhlax001@myuct.ac.za[2]

**ABSTRACT:** The integrity of majority of structures in Mount Moorosi village is undermined by the recurring cracks. However, no apparent institutionalized effort had been undertaken to identify the cause of this problem. The observed crack patterns are generally associated with the possible movements of the underlying loess-like soil. Therefore, it was herein imperative to study the structural arrangement of this soil using a Nova nano scanning electron microscope. Selected images were viewed at a magnification from 100x to 100000x. In addition, the hydrocollapse potential was experimentally investigated by performing a series of double oedometer (Global Digital System oedometer) tests. This was achieved by conducting tests on specimens at field moisture content and density, while other equally prepared samples were saturated. Micrographs revealed structures that synergistically augmented hydrocollapse of the soil. These were porous clays (kaolinite), silts (quartz and feldspar) coated with clay as well as silts bonded by clay, which all formed a metastable fabric. The measured hydrocollapse index at the applied stress of 200 kPa ranged from 9.6 to 15 %, while the collapse coefficient was from 0.13 to 0.18 at a vertical stress of 300 kPa. These results collectively demonstrated a soil which could possibly pose detrimental volume change and stresses to brittle masonry structures. The findings of this research could be used to explore the suitable ground improvement techniques, foundation designs and rehabilitation.

**Keywords:** loess-like; soil collapse; hydrocollapse; morphology

## *1. Introduction*

### *1.1. Background*

Howayek et al. (2012) defined loessal deposits as the most widespread collapsible soil covering approximately 10 % of the land area of the world. Pecsi (1990); Crouvi et al. (2010) reported its geographical distribution in Australia, Asia, Europe, the United States of America as well as in North Africa and Southern Africa (Namibia).

In loess, strength, mechanical behavior and other geotechnical properties are highly influenced by microstructural arrangement (that is morphology) of particles within a soil mass (Li et al., 2018). Figure 1 shows a structure of loess in which larger particles (that is sand and silt) are bonded by finer grains to form a porous matrix. The larger sized particles that remain unchanged in the presence of water are referred to as passive, while the finer cementing particles, which dissolve in water, are regarded as active.

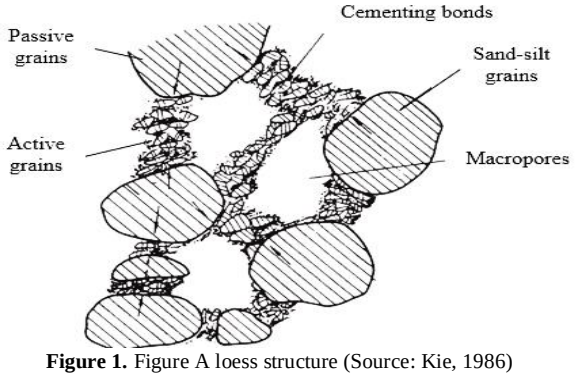


**Figure 1.** Figure A loess structure (Source: Kie, 1986)

Damane (2019) demonstrated that loess like deposits have relatively high shear strength at low moisture due to strong cementation, but drastically loose it under saturated conditions. This reduction in shear resistance increases soil susceptibility to settlement under applied loads. In soil mechanics, this water induced volume drop is termed hydrocollapse. It is documented in the literature (Djogo & Milović, 2013; Santrač et al., 2015 and Kalpakci, 2017) that this metastable fabric in loess makes it detrimental to structures. For this reason, understanding the morphology in a soil mass and hydrocollapse potential are imperative for designs of durable structures.

Several buildings in Mount Moorosi have sustained cracks which are potentially caused by the volume change of underlying loess like deposits. Therefore, this research aimed at investigating the soil particle arrangement, which renders the formation of a metastable structure. This was achieved by viewing a series of samples under a Scanning Electron Microscope (SEM). Furthermore, the hydrocollapse index was determined from the Global Digital System (GDS) oedometer. The results of this investigation were expected to show the soil structural arrangement and volume change properties which could be utilized in foundation designs.

### *1.2. Geological setting of study area*

Mount Moorosi is located 211.8 km south of Maseru in the Quthing district. It is situated at geographical coordinates of 30°16'39.76" S and 27°52'14.98" E in the Senqu River Valley agroecological zone in southern Lesotho. It is positioned at an elevation of 1700 m above mean sea level within the Clarens and upper Elliot of the Stormberg in the Karoo basin. Existence of mudrocks, siltstone and sandstone with over 3 m thick loess like deposits has been reported (Rooy & Schalkwyk, 1993; Damane, 2019). Figure 2 depicts the study area within the agroecological zones in southern Lesotho.

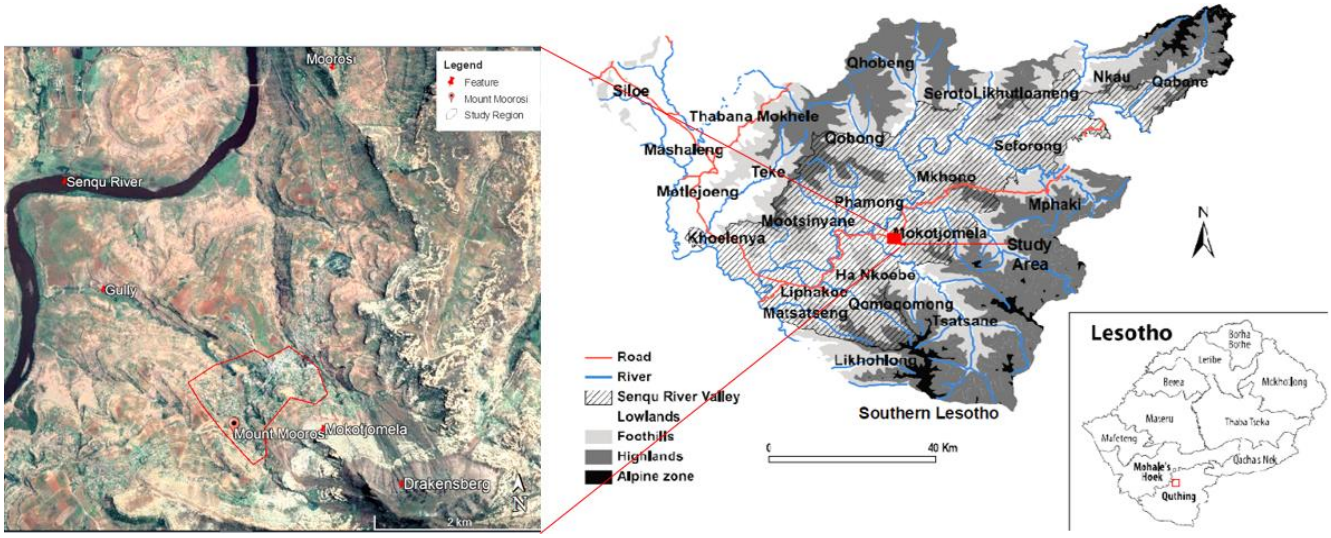


**Figure 2.** Study region in southern Lesotho (Source: Modified from Letsie, 2015)

## 2. Experimentation

### 2.1. Materials

The soil samples collected from the three trial pits in Mount Moorosi were taken to the geotechnical laboratory at University of Cape Town (UCT) for testing. Both the index and X-Ray Diffraction (XRD) tests were conducted for soil classification and mineralogy identification, respectively. The British Standard (BS 1377-2-1990) was adopted to execute the index tests. Field moisture and density were obtained using Troxler and were used to prepare the remolded oedometer specimens. The index and strength test results are summarized in Table 1.

**Table 1.** Summary of index and strength results of loess like deposits from Mount Moorosi Village (Source: Damane, 2019)

| Soil property | Site 1 | Site 2 | Site 3 |
|---|---|---|---|
| Specific gravity (g/cm$^3$) | 2.6 | 2.65 | 2.59 |
| Field moisture content (%) | 8.2 | 7.6 | 6.2 |
| Field bulk density (kg/m$^3$) | 1818 | 2021 | 1958 |
| Clay (%) | 9.7 | 8.0 | 12.0 |
| Silt (%) | 66.3 | 78.0 | 70 |
| Sand (%) | 23 | 12 | 18 |
| Liquid limit (%) | 33.0 | 28.7 | 26.0 |
| Plastic limit (%) | 16.0 | 14.7 | 14.0 |
| Plasticity index (%) | 17.0 | 14.0 | 12.0 |
| Linear shrinkage | 5.0 | 5.8 | 5.7 |
| Unified Soil Classification System | CL | CL | CL |
| Slaking rate | 3 to 4 | 2 to 3 | 4 |
| Consolidated undrained cohesion (saturated) (kPa) | 100 (20) | 61 (21) | 36 (21) |
| Consolidated undrained friction angle (saturated) (°) | 18 (13) | 21 (10) | 26 (14) |

The tested samples were predominantly silt-sized with content ranging from 66 to 78 %, followed by sand (12 to 23 %), while clay was the least (8 to 12 %). Furthermore, identification and quantification of minerals in XRD revealed the passive component to be predominant (quartz: 42 %, feldspar: 32 % and mica: 12 %), while the active ones were subordinate (kaolinite: 8 %, gibbsite: 3 %, carbonates: 1.1 %, gypsum: 0.64 %, goethite: 0.2 % and halite: 0.62 %). This proportion is conforming to that of loess proposed by Engri (1972) and Jeong et al. (2011). Moreover, the investigated samples had a reduction of up to 80 % in cohesion when moisture was increased from field content to saturated conditions. Contrarily, friction angle was decreased by up to 46 %. This change was attributed to the increased interparticle pores and higher lubrication when moisture content was augmented (that is, higher pore pressure).

### 2.2. Test procedure

#### 2.2.1. Scanning Electron Microscope

Structural arrangement of the representative samples was identified under a Nova nanoSEM. This analysis was conducted on intact as well as disturbed samples at the Centre for Imaging Analysis at UCT. Intact soil aggregates enabled the observation of wider range bonding, while disturbed grains clearly showed cementation between individual particles. The soil was gently sprinkled on SEM stubs that were provided with carbon glue on the surface. This was done in order to secure the soil during examination. The stubs were finally taken to a SEM for observation. A beam of electrons was focused on the soil to generate the micrographs. The viewing was at a magnification ranging from 100x to 100000x.

#### 2.2.2. Double oedometer test

Hydrocollapse potential was determined from an automated GDS double oedometer. The tests were performed on specimens reconstituted at in-situ density and moisture content, while other identical samples were equally prepared, but tested under saturated conditions. This experimentation demonstrated the behavior of a

loaded soil in both dry and rainy seasons and it provided an opportunity to analyze the water induced volume change. The British Standard method (BS 1377-5-1990) was followed during the tests execution.

Oedometer testing was carried out on a soil which was pre-watered to bring it to field moisture condition and left for a maturing age of 24 hours. It was initially compacted in a compaction mould based on BS 1377-4-1990; however, the soil crumbled when cut to fit the consolidation ring with a wire saw. Therefore, compaction was directly done in a consolidation ring to avoid unidentical specimens. The apparatus for soil preparation are demonstrated in Figure 3 ((a) shows consolidation ring bolted to compaction platform, while (b) demonstrates the compaction process).

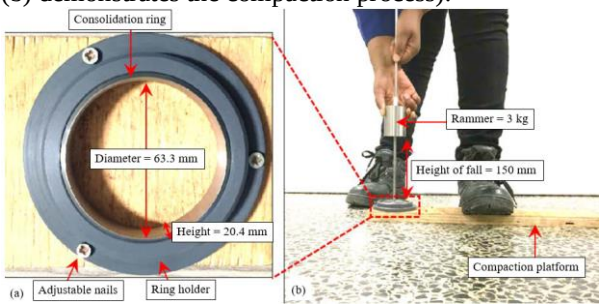


**Figure 3.** Sample preparation apparatus (Source: Damane, 2019)

Several trials were undertaken to achieve the predetermined field density in a consolidation ring. This involved varying the number of soil layers, height of fall and number of blows.

The first soil layer, with known mass, was uniformly spread inside a slightly oiled ring. The grease was used to minimise friction between the soil and ring. It was compacted with 3 kg rammer falling at a height of 150 mm. This layer was then scratched before the placement of the successive one to increase bonding between the soil. Table 2 summarizes height of fall, number of layers and blows in all the tested samples. When all the layers were compacted, total mass of the ring together with specimen was determined.

**Table 2.** Oedometer test compaction summary (Source: Damane, 2019)

| Sites | Test moisture state | Initial moisture content (%) | Number of layers | Number of blows |
|---|---|---|---|---|
| 1 | Natural | 7.8 | 3 | 7 |
| | Saturated | 7.8 | 3 | 7 |
| 2 | Natural | 7.5 | 4 | 9 |
| | Saturated | 7.5 | 4 | 9 |
| 3 | Natural | 6.6 | 3 | 8 |
| | Saturated | 6.6 | 3 | 8 |

For the final set-up, the porous plates were saturated by submerging them in boiling water for 15 minutes. They were then placed in cold distilled water for cooling. The bottom plate (95 mm in diameter and 9.5 mm in thickness) was placed inside the consolidation cell and gently aligned with a moist filter paper. The purpose of the paper was to prevent washing of soil particles into the pores of the plate. The compacted specimen was transferred onto the bottom plate and the second filter paper was sequentially placed on its surface. The top porous plate (60.5 mm in diameter and 10 mm in thickness), also provided with a metallic loading cap, was placed at the top of the specimen.

The consolidation cell was correctly aligned and bolted to achieve adequate lateral confinement. The piston was then lowered on the loading cap and a seating load of 2 kPa was applied. When the rate of change in settlement was constant (that is, in approximatelly 10 minutes), water was poured from the bottom to the brim of the cell. A seating load was left for a duration of 24 hours. The relatively small applied stress was selected to minimise subsidence during saturation stage.

A sequence of stresses (6, 12, 25, 50, 100, 200, 400, 800 and 1600 kPa) was each applied sequentially and held constant for 24 hours. According to BS 1377-5-1990, this duration was enough to achieve primary consolidation initiated by the applied loads. Furthermore, the higher loadings simulated the pressures from structures that could potentially be built in future in the study area, while the lower values were similar to those from typical buildings (<25 kPa). The live data was viewed and automatically recorded. At the end of the test, the oedometer was dismantled and water was drained from the cell. The final mass of the ring was meassured. The same procedure was followed in all the samples from various trial pits. However, in tests at in-situ moisture content, water was not added to the consolidation cell.

## *3. Results and discussion*

### *3.1. Scanning electron microscope*

The selected micrographs of samples from several pits in Mount Moorosi revealed the occurrence of various particle shapes. These included sub-angular, angular, platy and needle grains. Such forms were also reported on loess in North China and Rio Grande do Sul, Brazil (Derbyshlre et al., 1994; Lopes et al., 2016). The observed grains were predominantly silt-sized cemented and coated with finer particles to form aggregates. Figures 4 to 8 present these micrographs from SEM.

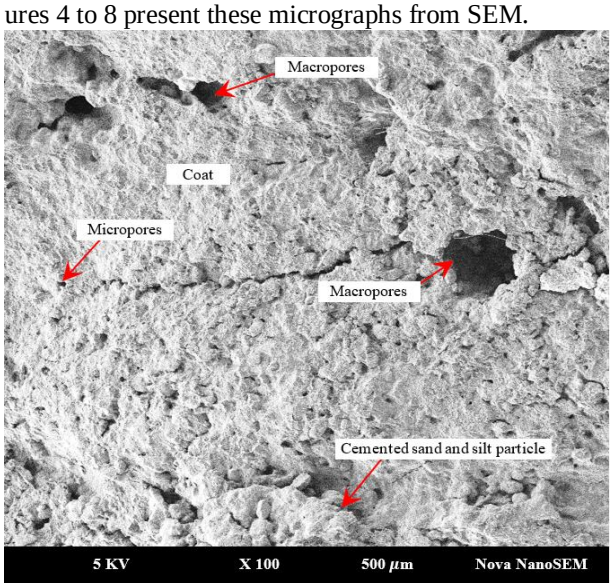


**Figure 4.** Intact SEM-micrograph showing particle cementation and pores, site 1 (Source: Damane, 2019)

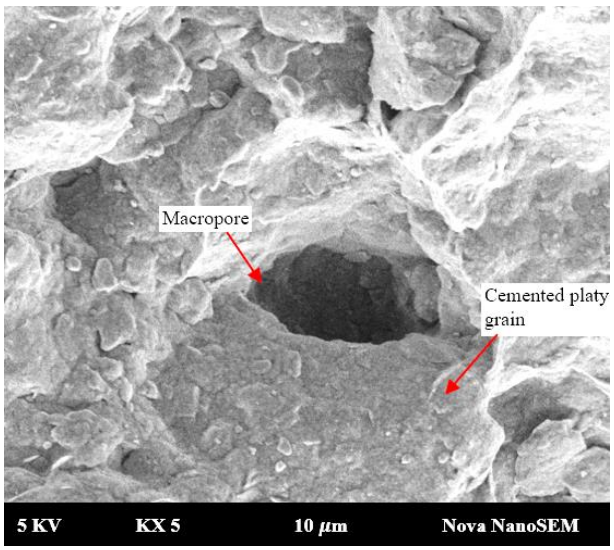


**Figure 5.** SEM-micrograph showing cemented particles to form a macropore, site 2 (Source: Damane, 2019)

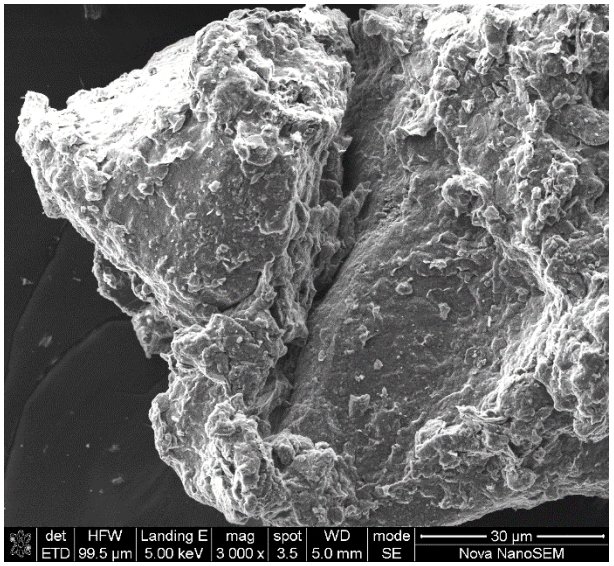


**Figure 6.** SEM-micrograph of bonding between two sub-angular particles, site 1 (Source: Damane, 2019)

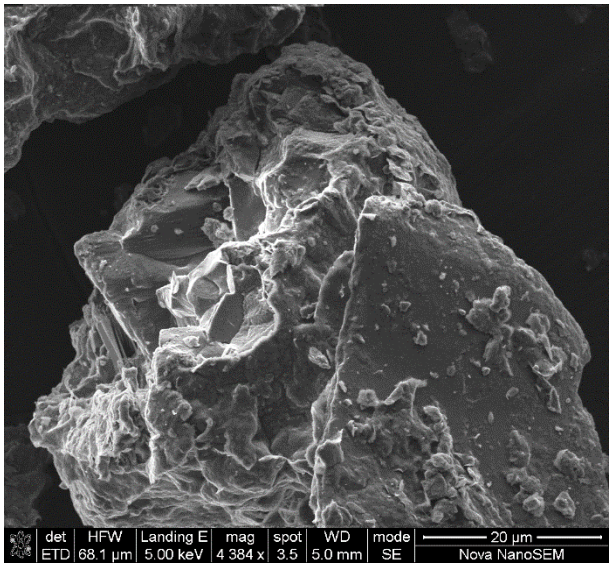


**Figure 7.** SEM-micrograph showing coating around angular and platy particles, site 1 (Source: Damane, 2019)

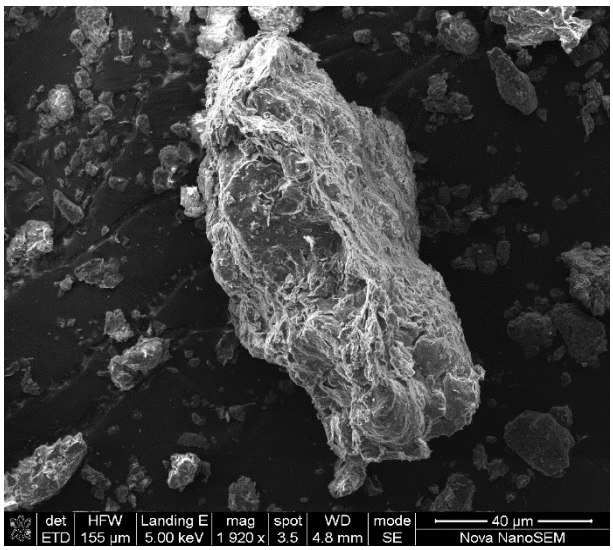


**Figure 8.** SEM-micrograph of a coated sub-angular particle, site 2 (Source: Damane, 2019)

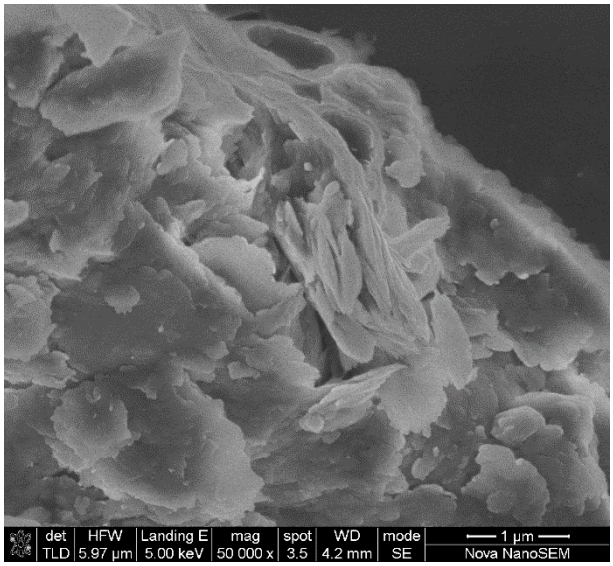


**Figure 9.** SEM-micrograph of kaolinite aggregation, site 3 (Source: Damane, 2019)

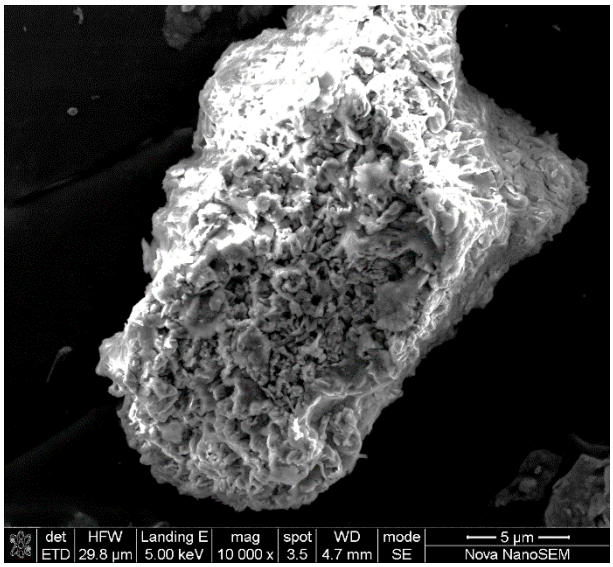


**Figure 10.** SEM-micrograph of tubular grains aggregation, site 3 (Source: Damane, 2019)

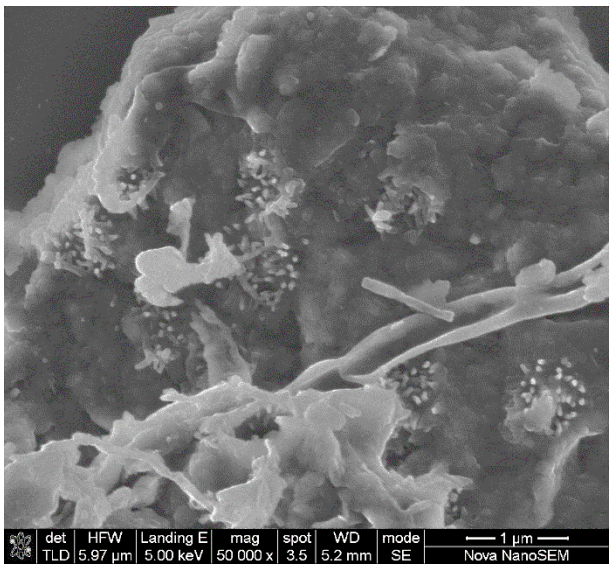


**Figure 11.** SEM-micrograph of needle calcite, site 1 (Source: Damane, 2019)

Figure 4 depicts an intact cohesive matrix formed by sand and silt sized particles that are coated by finer material. This soil structure demonstrates a clear distribution of both the macropores and micropores. Assallay (2001) reported that this open arrangement is an indication of possible hydrocollapse upon wetting of a loaded soil. According to Zhu (1963), such pores are caused by movements of plant roots. Contrarily, Brink (1985) attributed them to leaching of clay minerals from the soil. Ng et al. (2017), on the other hand, related them to the accumulation of clay minerals on the interparticle of sand and silt. Another macropore formed by flocculation of particles is shown in Figure 5.

Figure 6 is a micrograph of two silt-sized sub-angular grains that are bonded together. This type of bonding could be associated with relatively high shear strength parameters reported on Table 1 at low/field mosture content. The particle arrangement is similar to the conceptual model proposed by Kie (1986) for collapsible loess deposits (refer to Figure 1). This is an indication that the tested soil has structure comparable to that of loess from other parts of the world. Further cementation is depicted in Figure 7 in which both the platy and angular randomely orientated quartz grains are aggregated by a thin coat. A micrograph in Figure 8 demonstrates a silt particle which is submerged by kaolinite flakes. Barden et al. (1973) refers to such cementation as clay onion skin and attributes it to authigenesis process (that is formation of minerals at the same location in which they are found).

Figures 9 and 10 show an aggregation of kaolinite flakes and a porous tubular flocculation of grains, respectively. These cohabit with larger passive particles as infilling and possibly become active on saturation. The needle fibre calcite are also demonstrated in Figure 11. Such type of carbonates only exist in loess or fertile soil (Barta, 2011). They are soluble in water and could potentially contribute to hydrocollapse.

Generally, the morphological analysis revealed structures that could collectivelly initiate hydrocollapse settlement when the soil is saturated and loaded. Essentially, water weakens the strong interparticle bonds and could subsequently mobilize the passive grains.

## *3.2. Double Oedometer*

To determine the magnitude of potential hydrocollapse, a comparison of compression curves from tests at saturated and natural water contents was made. The consequent vertical offset (that is change in void ratio) between these curves was used in the analysis of soil susciptability to collapse. American Standard Testing Methods (ASTM-D5333-03) proposed that this change in void ratio is used in Equation 1 to establish the hydrocollapse index, $I_c$. The degree of possible damage to constructed structures was estimated from this index at an effective stress of 200 kPa (refer to Table 3).

$$I_c = \frac{\Delta e}{1+ e_o} \times 100 \quad (1)$$

Where, $\Delta e$ is the change in void ratio induced by inrease in moisture content and $e_o$ is the initial void ratio.

**Table 3.** Classification of the degree of hydrocollapse based on collapse index (Source: ASTM - D5333 - 03)

| Degree of hydrocollapse | Collapse index, Ic, (%) |
|---|---|
| None | 0 |
| Slight | 0.1 – 0.6 |
| Moderate | 2.1 – 6.0 |
| Moderately severe | 6.1 - 10 |
| Severe | >10 |

Lutenegger & Hallberg (1988) also proposed a collapse coefficient, *i*, for loess deposits at an applied stress of 300 kPa (refer to Equation 2). Based on this coefficient, the values greater than 0.02 are an indication of collapse problems to the superimposed structures.

$$i = \frac{\Delta e}{1+ e_1} \quad (2)$$

Where, $\Delta e$ is a change in void ratio due to wetting, $e_1$ is a void ratio prior to wetting.

ASTM-D5333-03 and Lutenegger & Hallberg (1988) procedures were adopted to analyze the degree of hydrocollapse settlement. Figures 13 to 14 presents the comparison graphical plots in samples from several pits in Mount Moorosi and the subsequent vertical offsets.

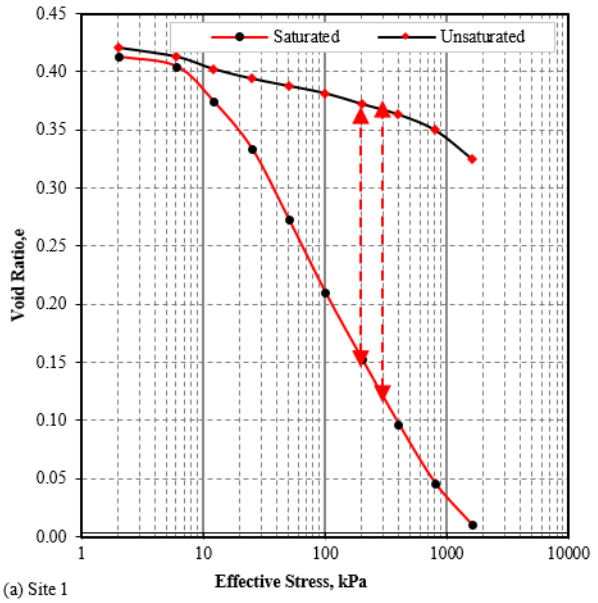


**Figure 12.** Comparison compression curves in samples from site 1 obtained from oedometer for determination of hydrocollapse (Source: Damane, 2019)

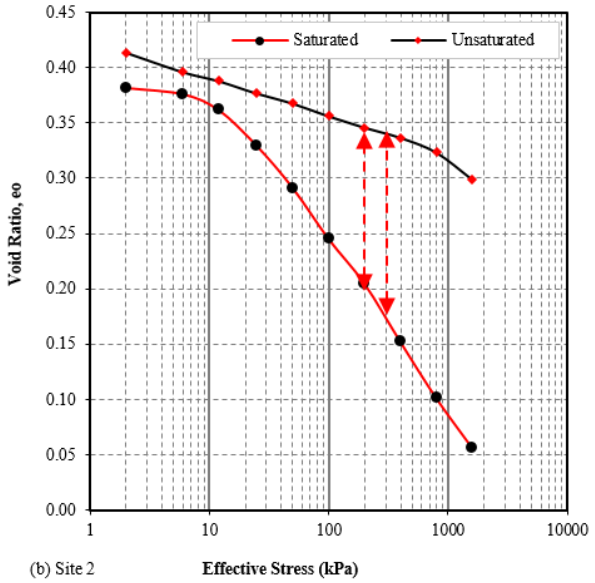


**Figure 13.** Comparison compression curves in samples from site 2 obtained from oedometer for determination of hydrocollapse (Source: Damane, 2019)

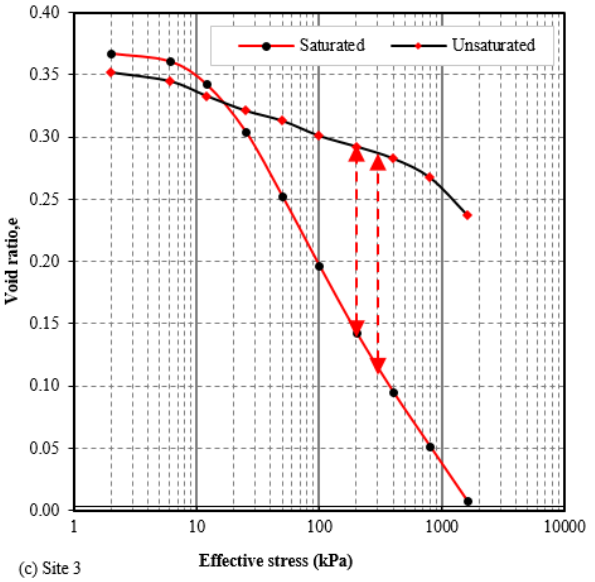


**Figure 14.** Comparison compression curves in samples from site 3 obtained from oedometer for determination of hydrocollapse (Source: Damane, 2019)

In all the tests, it was evident that at in-situ water content, the change in void ratio with increase in applied stress was relatively small compared to that in saturated conditions. The reason for this could be attributed to the sufficiently high shear strength parameters at low moisture (refer to Table 1), which enhanced particle interlocking and resistance to sliding. Essentially, the micrographs presented in section 3.1 demonstrated soil particles which appeared to be rigidly bonded. In fact, Assallay (2001) documented that at low water content, the clay bonding passive grains is slightly compressed by the vertical pressure resulting in minor volume decrease.

Under saturated conditions, the samples from site 1 and 2 demonstrated a small reduction in void ratio at lower applied stresses (that is, less 10 kPa). Contrarily, the soil from site 3 showed swelling, which was indicated by higher void ratio in saturated test than at natural moisture content. This was possibly caused by greater kaolinite composition (9.1 %), while others had lower values (that is 7.7 and 7.2 % for site 1 and 2, respectively). Nevertheless, a drastic decrease in void ratio concurrently occured with rise in vertical stress untill the tests were ended at 1600 kPa in all the samples. This was associated with the shear strength parameters which were reduced by up to 80 % due to wetting. Under such conditions, the lubrication caused by water initiated particles rearrangement and subsequent settlement. Furthermore, the structural disruption caused by slaking process (that is disaggregation of soil lumps into finer particles in water), exacerbated the soil collapse (refer to Table 3). A study conducted by Mbhele (2019) on Mount Moorosi loess like deposits also comfirmed high slaking tendency. This was initiated by rise in pore water and consequential rapid dessipation of air, which was indicated by bubbles (Damane, 2019). Liu et at. (2015) also reported that slaking enhanced collapse in loessal deposits.

Table 4 presents a summery of collapse index and coefficint for all the samples from several sites. It is observed that the degree of collapse classified as moderately severe to severe with collapse index ranging from 9.6 to 15.3 %. Assallay et al. (1996), Nouaouria et al. (2008) and Howayek et al. (2012) also documented similar values in loess from Libya, Algeria and Indiana, respectively. This indicated possibility of hydrocollapse problems to structures constructed on this soil. Besides, the collapse coefficient ranged from 0.13 to 0.18 on tested samples, which also showed a problematic soil.

**Table 4.** Collapse index and coefficient measured in samples from various sites

| Sample location | Effective pressure (kPa) | Collapse index, (%) | Collapse coefficient |
|---|---|---|---|
| Site 1 | 200 | 15.3 (severe) | |
| | 300 | | 0.18 |
| Site 2 | 200 | 9.6 (moderately severe) | |
| | 300 | | 0.14 |
| Site 3 | 200 | 10.7 (severe) | |
| | 300 | | 0.13 |

The variation of collapse potential and coefficient with increase in effective stress is demonstrated in Figure 15 and 16, respectively. Evidently, the graphs were flattening at pressures below 15 kPa, which indicated small water induced settlement. However, at stresses beyond 20 kPa, a significant collapse was shown by steepning. At greater stresses (that is above 800 kPa), reduction in collapse was demonstrated by the curves which became flat.

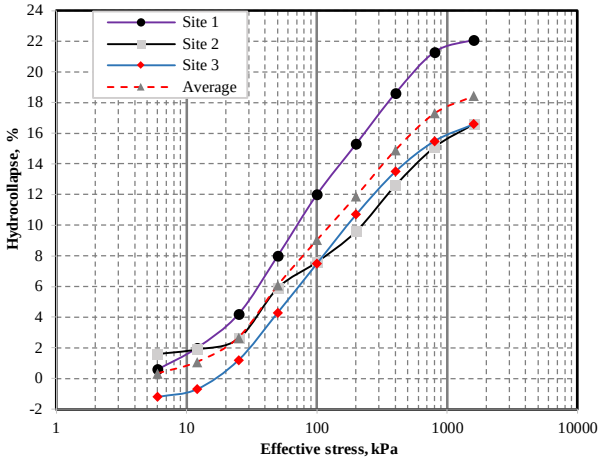


**Figure 15.** Variation of hydrocollapse with rise in effective stress

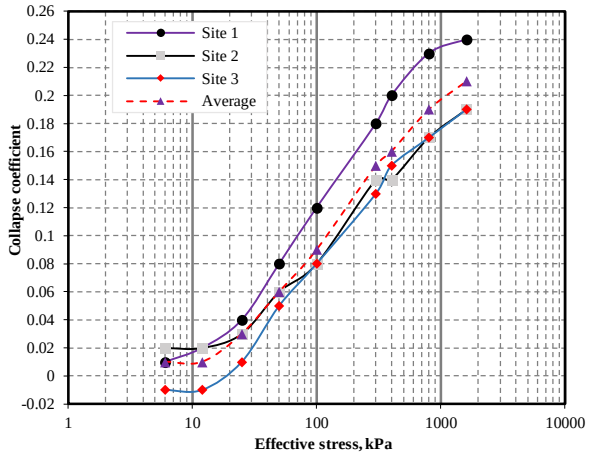


**Figure 16.** Variation of collapse coefficient with rise in effective stress

## *4. Conclusion*

From the determination of morphology and hydrocollapse behavior of the soil in Mount Moorosi, it was established that: the structural arrangement consisted of angular, sub-angular and platy sand and silt-sized particles. These grains were predominantly bonded by clay to form a porous fabric.

The soil had a moderately severe to severe hydrocollapse potential with values ranging from 9.6 to 15.3 %, while the collapse coefficint was from 0.13 to 0.18. The morphology and magnitude of water induced collapse collectively indicated a problematic soil. The findings of this research could be used for rehabilitation, foundation designs and to explore suitable ground improvement techniques.

## *5. References*


[1] American Standard Test Methods (ASTM D5333 – 03 – 1996), Standard Test Method for Measurement of Collapse Potential of Soils.

[2] Assallay, A.M., Rogers, C.D.F. & Smalley, I.J. Engineering properties of loess in Libya: Journal of Arid Environments, Vol. 32: 373–386. 1996.

[3] Assallay, A. m. Structure and Hydrocollapse Behaviour of Loess. Doctoral Thesis: Loughborough University Institutional Repository. 2001.

[4] Crouvi, O., Amit, R., Enzel, Y. & Gillespie, A. R. Active Sand Seas and the Formation of Desert Loess. Quaternary Science Reviews, Vol. 29: 2087 - 2098. 2010.

[5] Barden, L., McGown, A. & Collins, K. The Collapse Mechanism in Partly Saturated Soil. Engineering Geology, Vol. 7: 49 - 60. 1973.

[6] Barta, G. Secondary Carbonates in Loess-Paleosoil Sequences: A General Review. Central European Journal of Geosciences, Vol: 3(2): 129 - 146. 2011.

[7] British Standard (BS 1377-2-1990). Methods of test for Soils for civil engineering purposes, Part 2: Classification tests.

[8] British Standard (BS 1377-4-1990). Methods of test for Soils for civil engineering purposes, Part 4: Compaction-related tests.

[9] British Standard (BS 1377-5-1990). Methods of test for soils for civil engineering purposes. Compressibility, permeability and durability tests, Part 5: Compaction-related tests.

[10] Damane, M. An investigation into the volume change characteristics of loess like deposits in Mount Moorosi Village in Lesotho. Master's dissertation: University of Cape Town. 2019.

[11] Derbyshlre, E., Meng, X., Wang, J., Zholf, Z. & Li, B. Collapsible Loess on the Loess Plateau of China. Genesis and Properties of Collapsible Soils. Loughborough, U.K. 1994.

[12] Djogo, M. & Milović, D. Differential settlement of foundations on loess. Seventh international conference on case histories in geotechnical engineering. Missouri University of Science and Technology. 2013.

[13] Egri, G. The Physico-Chemical Properties and Engineering Problems of the Loess Soils. Acta Gelo. Acad, Sci. Hung, Vol. 16: 337 - 345. 1972.

[14] Howayek, A.E.I., Huang, P., Bisnett, R. & Santagata, M.C. Identification and Behavior of Collapsible Soils, Joint transportation research program, FHWA/IN/JTRP-2011/12. 2011.

[15] Jeong, G. Y., Hillier, S. & Kemp, R. B. Changes in Mineralogy of Loess–Paleosol Sections Across the Chinese Loess Plateau. Quaternary Research, Vol. 75: 245 - 255. 2011.

[16] Kalpakci, V. Collapse of Base Soil and its Consequences During a Cement Plant Construction. Selcuk University Journal of Engineering, Science and Technology, Vol. 5: 500 -510. 2017.

[17] Kie, T. T. Fundamental Properties of Loess from Northwestern China. Engineering Geology, Vol. 25: 103 - 122. 1986.

[18] Li, Y., He, S., Deng, & Xuc, Y. Characterization of Macropore Structure of Malan loess in NW China Based on 3D Pipe Models Constructed by Using Computed Tomography Technology. Journal of Asian Earth Sciences, Vol 154: 271 - 279. 2018.

[19] Liu, Z., Liu, F., Ma, F., Wang, M., Bai, X., Zheng, Y., Yin, H. & Guoping Zhang, G. Collapsibility, Composition, and Microstructure of a Loess in China. Canadian Geotechnical Journal, Vol. 53 (4): 673 - 686. 2015.

[20] Lopes, R. P., Dillenburg, S. R, & Schultz, C. L. Cordão Formation: Loess Deposits in the Southern Coastal Plain of the State of Rio Grande Do Sul, Brazil. Anais da Academia Brasileira de Ciências, Vol. 88: 2143 - 2166. 2016.

[21] Lutenegger, A.J. & Hallberg, G.R. Stability of Loess. Engineering Geology, Vol. 25: 247 – 261. 1988.

[22] Mbhele, M. An Investigation into the Erodibility of Loess-like Soils in Mount Moorosi Village in Lesotho. Undergraduate dissertation: University of Cape Town. 2019.

[23] Ng, C. W. W., Mu, Q. Y. & Zhou, C. Effects of Soil Structure on the Shear Behaviour of an Unsaturated Loess at Different Suctions and Temperatures. Canadian Geotechnical Journal, Vol. 54 (2): 270 - 279. 2017.

[24] Nouaouria, M. S., Guenfoud, M. & Lafifi, B. Engineering Properties of Loess in Algeria. Engineering Geology, Vol. 99: 85 - 90. 2008.

[25] Santrač, P., Bajić, Z., Grković, S., Kukaras, D. & Hegediš, I. Analysis of Calculated and Observed Settlements of the Silo on Loess, Tehnički vjesnik, Vol. 22: 539-545. 2015.

[26] Pecsi, M. Loess is Not Just the Accumulation of Dust. Quaternary International, Vol. 7/8: 1 - 21. 1990.

[27] Rooy, J. L. V. & Schalkwyk, A. V. The geology of the Lesotho Highlands Water Project with Special Reference to the Durability of Construction Materials. Journal of African Earth Sciences, Vol. 16: 181-192. 1993.

*Acknowledgement*

The project presented in this article is supported by MasterCard Foundation Programme at the University of Cape Town.